Paper presented at the 34th International Conference and Exhibition of ICSOBA
(International Committee for Study of Bauxite, Alumina & Aluminium)
Québec, Canada, October 3-6, 2016

The influence of tool geometry on mechanical properties of friction stir welded AA-2024 and AA-2198 joints

Mahdi Masoumi[1], Yasser Zedan[2], Damien Texier[3], Mohammad Jahazi[4], and Philippe Bocher[5]
1. MSc. Student
2, 3. Research Assistant
4, 5. Professor
Aluminium Research Centre-REGAL, École de technologie supérieure, Montreal, Canada
Corresponding author: mahdimasoumi90@gmail.com

Abstract

The tool geometry in friction stir welding (FSW) is a critical parameter to produce reliable and consistent joints, especially when it comes to joining dissimilar alloys with different mechanical and thermal properties. The aim of the present work is to investigate the effect of FSW tool design on the mechanical characteristic of as-welded AA2198(T3)-AA2024(T3) joints. Three shoulder profiles (flat, spiral, and fan) and five different pin profiles (tapered cylindrical, straight cylindrical, threaded cylindrical, cone and square) were tested. A visual inspection and metallographic characterization were conducted to evaluate the sound state of the joint. Tensile tests and scanning electron microscopy combined with energy-dispersive X-ray spectroscopy were used to assess the mechanical properties of the different joints in regard to fractographic analyses and local chemical composition. Significant flash was produced for flat shoulder configurations. FSW tools with fan or with spiral shoulders prevent the formation of the flash defect. Lack of penetration (LOP) and kissing bond defects were avoided by tapering the tip of the pin with a diameter greater than or equal to the plate thickness. The tapered cylindrical pin with a fan shoulder was the optimal tool design configuration for mechanical properties.

Keywords: FSW tool design; friction stir welding; Al-Li alloys; 3rd generation aluminum alloys; 2024 aluminum alloy.

1. Introduction

Developing advanced alloys with superior mechanical properties and new manufacturing processes is essential for the aerospace industry. Recently developed aluminum alloys, such as the AA-2198 Al-Li alloy, emerged to improve the mechanical properties and lower density of their conventional counterparts, e.g., AA-2024 [1]. However, these benefits come at the expense of higher material cost. Therefore, an economical solution is to use AA-2198 alloys only for critical regions/components, with the remaining structure retaining AA-2024 alloys. A method for to joining these dissimilar materials is therefore needed. Unfortunately, conventional fusion welding methods are not appropriate solutions as they result in welding defects, such as hot cracking [2].
Friction Stir Welding (FSW) is a solid-state welding technique that has evolved as a solution for joining dissimilar materials that are difficult to weld [3]. It is currently used as an alternative to riveting for the assembly of airplane fuselages. FSW uses a rotary pin to locally mix the materials of the two sides of the joint below the melting point temperature. Thus, the formation of welding defects such as hot cracking is prevented.
Selecting appropriate FSW tool and process parameters is essential for creating a reliable joint in aerospace applications, especially for joining dissimilar alloys with different mechanical and thermal properties. Both the shoulder and pin profiles are important for having a defect-free joint. The optimization of either the shoulder [4-6] or the pin design [7-11] for FSW tools has

been reported in the literature for producing joints with optimum mechanical properties. L. Trueba Jr. et al. [6] showed that the fan shoulder has a great potential for producing high quality welds, even under non-ideal process conditions. K. Krasnowski [12] showed that cylindrical pins with and without thread are capable of producing defect-free joints for AA-6082-T6 aluminum alloys. The effect of pin geometry on the mechanical properties of FSWed 2014 aluminum alloy was also reported by Zhao et al. [13]. They found that the optimum weld quality was obtained by using the taper pin with a screw thread.
The last generation of aluminum alloys comprises relatively new materials, and tool design optimization for these materials required particular investigation. Among the few works conducted on the FSW of dissimilar aluminum alloys, Velotti and Astarita reported critical technological challenges facing FSW for lap joints of AA-2198-T351 and AA-7075-T6 alloys [14] and T-shaped joints of AA-2198-T3 and AA-6056-T4 [15]. Dissimilar friction stir welded butt joints made of AA-2024-T3 and AA-2198-T3 have already been investigated in terms of microstructural and specific mechanical characterizations [16, 17]. In this study, the effect of tool shoulder and pin profile on the microstructure and mechanical properties of FSWed AA-2024-T3/AA-2198-T3 joints were documented right after welding, without any natural aging. To that end, three different shoulder and five tool pin profiles were used to fabricate the joints, while the other welding parameters were kept constant.

2. Experimental

2.1. Tool design

The possibilities in tool design are endless, but the combinations of shoulder and pin profiles are crucial for the quality of the finished weld. A comprehensive literature review was carried out in order to determine relevant choices for the tool design. A review of all the selected design parameters is detailed in Table 1 [5, 6, 18-22]; based on this review, seven tool configurations denoted from A to G in Figure 1 were designed and manufactured to evaluate the quality of the joint. Because information on the minimal pin diameter in the tapered pins at the welding joint was lacking in the literature, the effect of this parameter is also evaluated in the present study (Table 1).

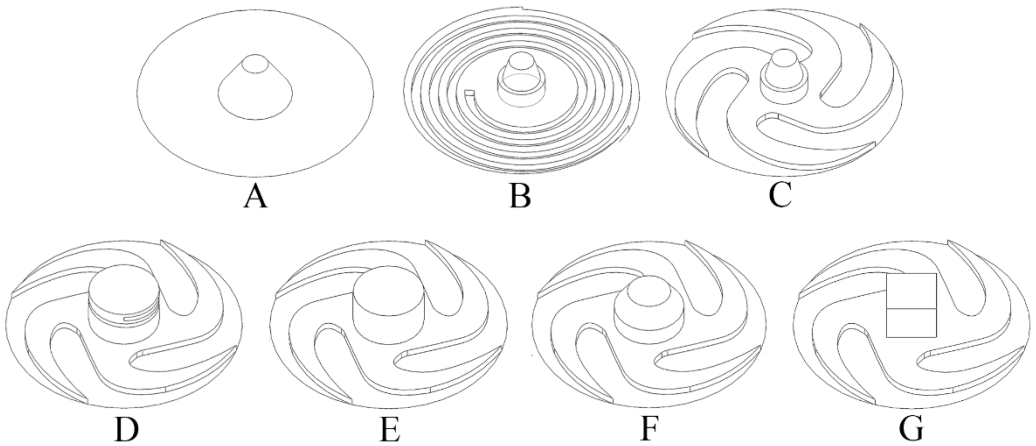

Figure 1. Tool configurations: (A) Flat shoulder with conical pin, (B) Spiral shoulder with stepped conical pin, (C) Fan shoulder with stepped conical pin, (D) Fan shoulder with threaded cylindrical pin, (E) Fan shoulder with cylindrical pin, (F) Fan shoulder with tapered cylindrical pin, (G) Fan shoulder with cubic pin.

Table 1. Selected parameters for FSW tool design.

Parameter	Tool design parameters from the literature	Types
Tool material	AISI 4340 [18]	All
Tool Shoulder Diameter	2.2*Plate thickness (mm) + 7.3 [18]	All
Pin length	Up to 0.3 mm smaller than plate thickness [19]	All
Max outer pin Diameter	Plate thickness [20]	A, B and C
	0.8*Plate thickness (mm)+2.2 [18]	D, E, F and G
Min-pin Diameter	0.5 * plate thickness	A, B and C
	Equal to plate thickness	F
Shoulder profile	Spiral shoulder [18]	B
	Raised fan shoulder [6]	C, D, E, F and G
Pin profile	Stepped conical pin [20]	B and C
	Half-screw pin [21]	D
	Straight cylindrical pin [5]	E
	Square pin [22]	G

2.2. Materials and methods

The base materials used in the present investigation are AA-2024-T3 and AA-2198-T3 rolled sheets with a thickness of 3.2 mm. The nominal chemical compositions of these base materials are reported in Table 2. Figure 2-a depicts the FSW process setup. The configuration used was chosen based on the fact that the tensile properties of AA2198-T3 in the rolling direction are similar to those of AA2024-T3 in the transverse direction. In the case of dissimilar joints, AA-2024 and AA-2198 plates were placed on the retreating side and on the advancing side, respectively. The weld was perpendicular to the AA-2198 rolling direction and parallel to the AA-2024 rolling direction [16]. The rotation speed, the welding advancing speed, the plunge depth and tilt angle were 750 RPM, 50 mm/min, 0.2 mm and 0 degree, respectively [23]. To ensure that the mismatch between plate edges has no effect on the formation of defects within the joints and that any defects present would only be related to the tool design, all tools were first tested using the 2024-T3 plates. Tools that did not produce any defects such as kissing bonds, flash, and tunneling defects, on the basis of metallography and eye examination were selected for the dissimilar welding of AA-2024 and AA-2198. Samples for further metallography and mechanical tests were extracted from the locations shown in Figure 2-b.

Table 2. Chemical compositions of AA2024 and AA2198 alloys in wt.% [24, 25].

Alloy	Cu	Li	Mg	Ag	Mn	Fe	Zn	Si	Ti	Al.
AA2024	3.8-4.9	-	1.2-1.8	-	0.3-0.9	≤0.5	0.2	≤0.5	0.15	Bal.
AA2198	2.9-3.5	0.8-1.1	0.25-0.8	0.1-0.5	≤0.5	≤0.01	≤0.35	≤0.08	-	Bal.

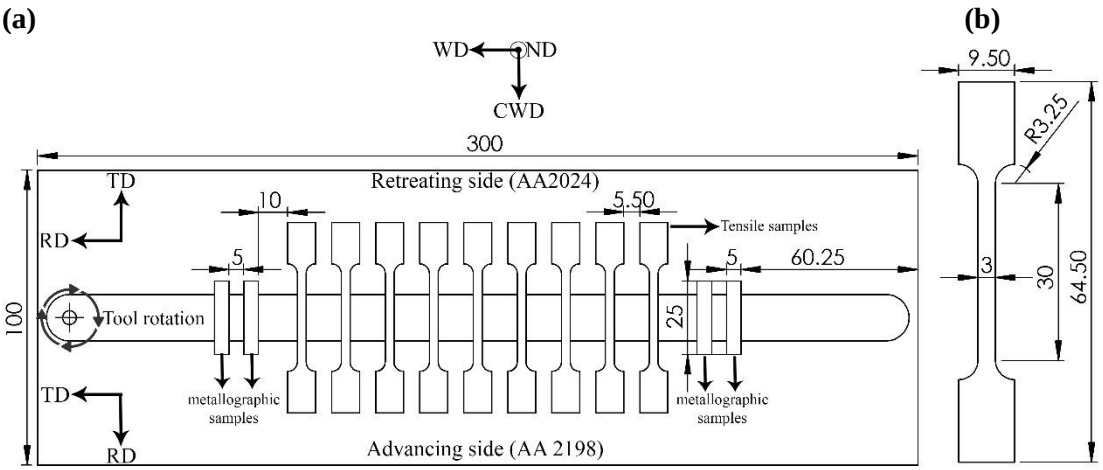

Figure 2. (a) Experimental dissimilar friction stir welding process setup and location of sample extraction (RD: rolling direction, TD: transverse direction, WD: welding direction, CWD: cross weld direction, ND normal direction); (b) Geometry of the macro-tensile samples. The all dimensions are in millimeters.

To reveal the microstructure, Keller etchant (2 mL HF (48%), 3 mL HCl (conc.), 5 mL HNO_3 (conc.), and 190 mL H_2O) for 15 s were employed after standard polishing down to 1 µm diamond paste and BUEHLER Vibromet2 for 48 h with 0.05 µm colloidal silicon solution. The joint microstructures were observed on ND-CWD plane. Optical micrographs were obtained with an OLYMPUS Lext OLS4100 laser scanning confocal microscope. A Hitachi SU-8230 scanning electron microscopy (SEM) with Energy-Dispersive X-ray Spectroscopy (EDS) was used to analyze the local chemical composition of the joint. Mechanical characterizations were performed on dog-bone tensile specimens with geometries as shown in Figure 2-b. They were machined from the welded plates such that the loading direction corresponded to the cross-welding direction of the joined plates. Specimens were extracted both from the joint (the joint being centered in the specimen gage) and from the base materials for references. Tensile tests were conducted on a 5kN Kammrath & Weiss micro-tensile device at a constant crosshead displacement rate of 7 $\mu m.s^{-1}$; i.e., a strain rate of approximately $2.3x10^{-4}s^{-1}$. The specimen elongation along the loading direction was continuously recorded using a Keyence LS-7030M optical extensometer sampling the extremities of the TMAZ regions (L_0=16mm). After testing, fracture surfaces were analyzed by SEM fractography.

3. Results

Metallography and visual examination results corresponding to the occurrence of kissing bond, tunneling defects and flash formation on the welded AA-2024-T3 joints are summarized in Table 3. The results found show that a flat shoulder (tool A) leads to flash formation on the welding surface. This outcome can be related to the fact that the flat shoulder is characterized by material flow from the edge to the center, which in turn results in flash formation. The tools used, having min-pin diameters half of the plate thickness (tools A, B and C), are responsible for the kissing bond defect. When this dimension is equal to the plate thickness (tools D, E, F and G), no kissing bond defect is present. This phenomenon can be related to the fact that a bigger min-pin diameter provides enough material flow at the root of the weld to join the materials. The results of the half-threaded cylindrical pin (tool D) shows a tunneling defect, which can be the result of high turbulent flow in the joint. Based on this evaluation, only tools E, F and G were able to create defect-free joints, and they were selected for use in joining AA 2024-T3 and AA 2198-T3.

A metallographic examination of the joints between AA 2024-T3 and AA 2198-T3 confirmed that defect-free joints were obtained using tools E, F, and G.

Table 3. Defects produced as a result of tool design.

Tool	Kissing Bond	Flash	Tunneling Defect
A	×	×	×
B	×		
C	×		
D			×
E, F and G	Defect-free		

The microstructures of the two base metal alloys are detailed in Ref. [16]. Cross-sectional observations of joints produced by tools E, F and G in on ND-CWD plane are shown in Figure 3. All the micrographs show that tracking the boundaries between the base metal, HAZ, and TMAZ using contrast, grain size, and morphology is difficult (Figure 3). On the one hand, the transition between the base metal and nugget regions on the AA-2198 side is straightforward to identify as a result of the appearance of small recrystallized grain microstructures. On the other hand, a transition band, rather than a singular boundary, was found on the AA-2024 side of the band, which is difficult to track exactly. Moreover, it is clear that differentiating the HAZ from the TMAZ based on microstructural reflection is impossible. It should be noted that the nugget encompasses two different zones divided by an S-shape border where a fine recrystallized microstructure on both sides of this border can be observed. This observable border could result from the grain size difference on both the sides of the border. Figure 4 depicts the energy dispersive spectroscopy (EDS) map on both sides of the S-shape border of Figure 3-a, where the difference in Mg content is significant. Comparing Table 2, which contains the chemical composition of the base metals, with the Figure 4, where the left side of the border shows a much higher amount of Mg than the right side, demonstrates that the left and right sides of the border are AA-2024 and AA-2198 metals, respectively. Therefore, it can be deduced that the nugget region encompasses non-mixed materials. Moreover, as can be seen in Figure 3-a, there is a sharp interface part along the border, between the two dissimilar materials in the metallography test. This phenomenon could be related to the turbulent material flow due to the centrifugal force of the end pin in the mixing area. Therefore, to assess the min-pin diameter, the results of tool F are depicted in Figure 3-b. This figure shows that the irregular sharp interface using this tool transforms to a smoother interface. This irregularity can be avoided by tapering the tip of the pin, just as tool F. However, considering the kissing bond and LOP defects, the end pin should have a diameter greater than or equal to the plate thickness, as previously shown in Table 3.

The ratio between the cross-section of the weld nugget (the area between two yellow lines in Figure 3 a and b) and the pin cross-section shows the ability of the tool to mix both materials, as shown in
Figure 5. Results show that tool F performs better in mixing both materials, as compared to the other tools.
The elongation, yield strength and ultimate tensile strength in the as-weld condition are shown in Figure 6. Results indicate that there is a negligible difference in the ultimate tensile strength for the different tool designs, but the tool F joint demonstrates a higher yield strength and elongation. Therefore, the tool F joint is an optimized tool design for the FSW of AA2024 and AA2198.

←AA 2024-RS
TD

AA 2198-AS→
RD

(a)

(b)

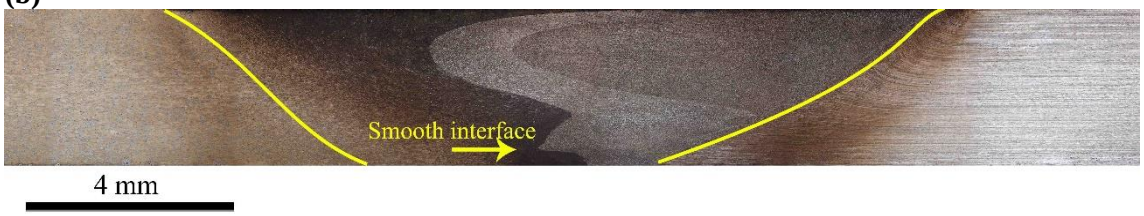

(c)

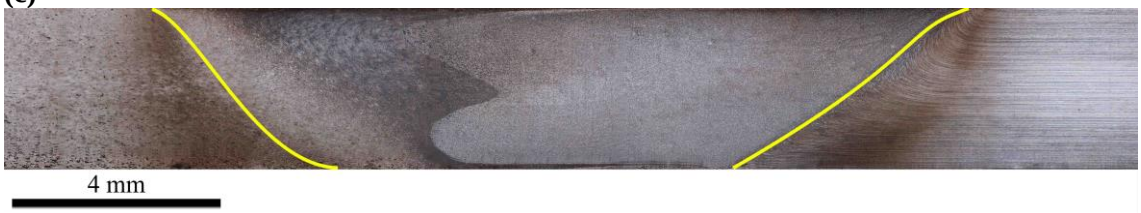

Figure 3. Cross-sectional observations of joints in ND and CWD planes: (a) tool E, (b) tool F, and (c) tool G.

AA 2024-RS 2198-AS

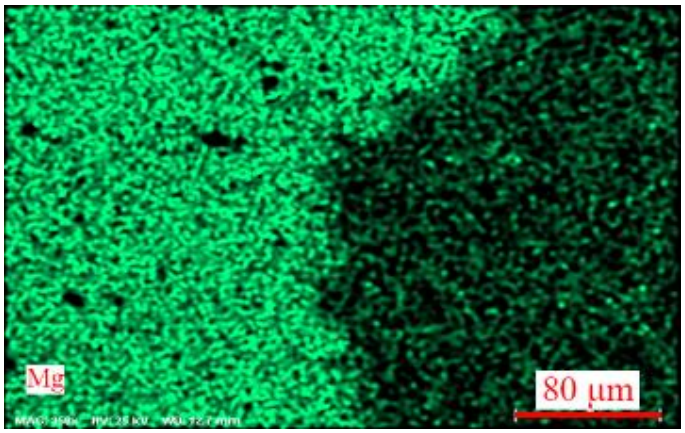

Figure 4. Energy dispersive spectroscopy (EDS) map inside the yellow rectangular in Figure 3-a (tool F).

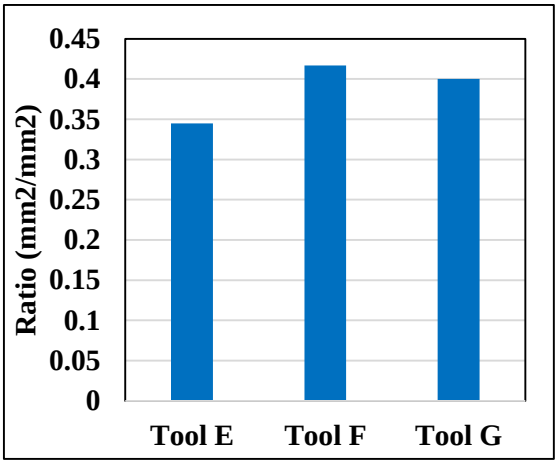

Figure 5. Ratio between pin and weld nugget cross-sections.

Particular attention was paid to the tool F tensile specimen due to its slightly higher ductility in the as-weld condition. The final fracture occurred in the nugget region close and parallel to the TMAZ on the AA-2024 retreating side, as show in Figure 7. Fractographic analyses were performed via scanning electron microscopy (SEM), and fracture surfaces depict typical features representative of ductile and trans-granular fracture, as shown in Figure 8-b. 5 to 10-µm large dimples are found on the whole fracture. The location of the fracture in the TMAZ/nugget region can be a result of the high welding temperature due to the high "rotation speed/advancing speed" ratio or to stress concentration related to the presence of the sharp edge created by tool plunge.

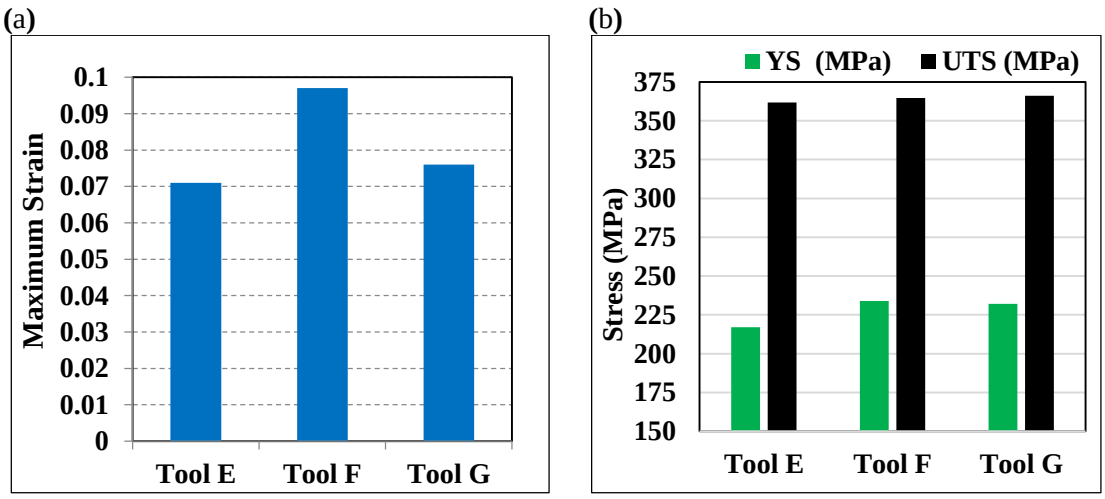

Figure 6. Mechanical properties of FSW joints produced by tools: (a) maximum strain, (b) 0.2 offset yield strength (YS), and ultimate tensile strength (UTS) (MPa).

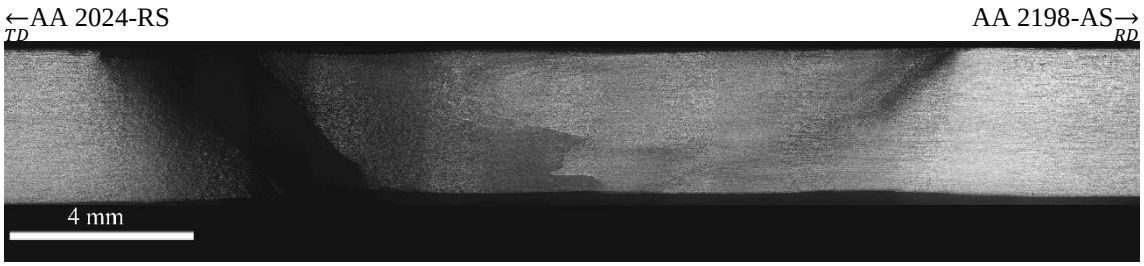

Figure 7. Final fracture of the joint produced by tool F in ND and CWD plane shows the location of the fracture is between the TMAZ and nugget region.

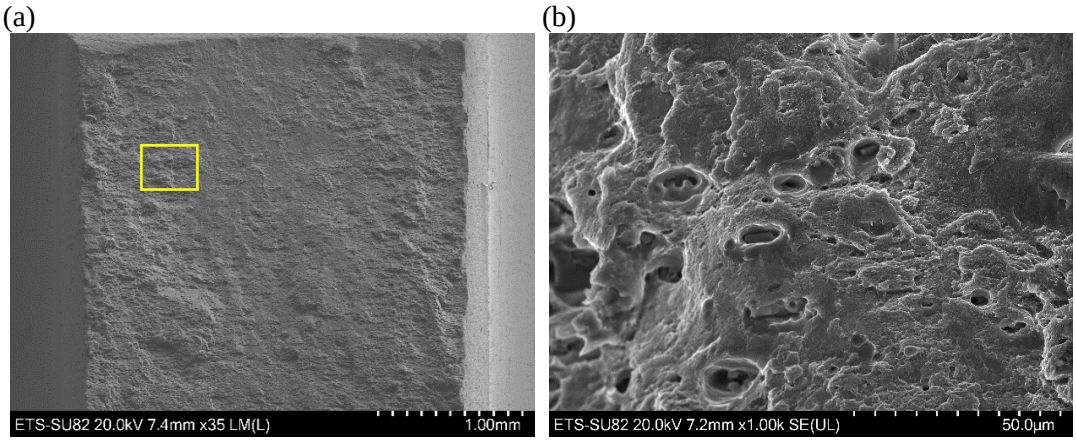

Figure 8. Fracture surfaces of the joint produced by tool F observed by SEM: (a) Low Magnification, (b) High magnification image of the yellow rectangular zone, show a ductile and trans-granular fracture.

4. Conclusions

The present study covers the effect of the FSW tool design on the mechanical characteristics of AA-2198/AA-2024 dissimilar joints. Five different pin profiles (tapered cylindrical, straight cylindrical, thread cylinder, cone and square) with three different shoulder profiles (flat, spiral, and fan) were designed and manufactured. Defect-free joints performed with these tools were characterized by means of visual inspection, metallographic images, tensile tests and fractography. The following are the main conclusions from the study:

- Tools with flat shoulders create flash defects.
- Spiral and fan shoulders prevent the formation of flash defects.
- Sharp interfaces between two dissimilar materials can be avoided by tapering the tip of the pin.
- The min-pin diameter plays an important role for LOP and kissing bond defects. The min-pin diameter must be greater than or equal to the plate thickness in order to avoid LOP defects.
- The tapered cylindrical pin with a fan shoulder joint exhibits better mechanical properties for FSW of AA-2198-T3 and AA-2024-T3. The fracture surfaces provided by this tool correspond to a ductile and trans-granular fracture.

5. Acknowledgment

We would like to express our appreciation to Eric Marcoux and Michel Orsini for their helps during this research. Without their valuable assistance, this work would not have been completed. A part of the research presented in this paper was financed by the Fonds de recherche du Québec – Nature et technologies by the intermediary of the Aluminium Research Centre – REGAL.

6. References

1. Nikolaos D. Alexopoulos et al., Fatigue behavior of the aeronautical Al-Li (2198) aluminum alloy under constant amplitude loading, *International Journal of Fatigue*, 2013. **56**(0), 95-105.
2. ASM Handbook and Brazing Welding, Soldering, vol. 6, *ASM International, Material Park, OH*, 2005, 438.
3. Rajiv Sharan Mishra and ZY Ma, Friction stir welding and processing, *Materials Science and Engineering: R: Reports*, 2005. **50**(1), 1-78.
4. A. Scialpi, L. A. C. De Filippis, and P. Cavaliere, Influence of shoulder geometry on microstructure and mechanical properties of friction stir welded 6082 aluminium alloy, *Materials & Design*, 2007. **28**(4), 1124-1129.
5. H. K. Mohanty et al., Effect of tool shoulder and pin probe profiles on friction stirred aluminum welds — a comparative study, *Journal of Marine Science and Application*, 2012. **11**(2), 200-207.
6. Luis Trueba Jr. et al., Effect of tool shoulder features on defects and tensile properties of friction stir welded aluminum 6061-T6, *Journal of Materials Processing Technology*, 2015. **219**(0), 271-277.
7. R Ashok Kumar and MR Thansekhar. *Effects of tool pin profile and tool shoulder diameter on the tensile behaviour of friction stir welded joints of aluminium alloys*. in *Advanced Materials Research*. 2014. Trans Tech Publ.
8. Mohd Hasbullah Idris and Mohd Shamsul Husin, Effect of Friction Stir Welding pin Shape on Mechanical Properties of AA6061 Alloy Weldment, *Applied Mechanics and Materials*, 2014. **465**, 1309-1313.
9. Md Reza-E-Rabby and Anthony P. Reynolds, Effect of Tool Pin Thread Forms on Friction Stir Weldability of Different Aluminum Alloys, *Procedia Engineering*, 2014. **90**(0), 637-642.
10. Saeid Amini and M. R. Amiri, Pin axis effects on forces in friction stir welding process, *The International Journal of Advanced Manufacturing Technology*, 2015, 1-7.
11. Ameneh Amirafshar and Hesam Pouraliakbar, Effect of tool pin design on the microstructural evolutions and tribological characteristics of friction stir processed structural steel, *Measurement*, 2015. **68**(0), 111-116.
12. K. Krasnowski and S. Dymek, A comparative analysis of the impact of tool design to fatigue behavior of single-sided and double-sided welded butt joints of EN AW 6082-T6 alloy, *Journal of Materials Engineering and Performance*, 2013. **22**(12), 3818-3824.
13. Yan-hua Zhao et al., The influence of pin geometry on bonding and mechanical properties in friction stir weld 2014 Al alloy, *Materials Letters*, 2005. **59**(23), 2948-2952.
14. C. Velotti et al. *On the critical technological issues of friction stir welding lap joints of dissimilar aluminum alloys*. 2013. Southern Gate, Chichester, West Sussex, PO19 8SQ, United Kingdom: John Wiley and Sons Ltd.
15. A. Astarita et al., On the critical technological issues of friction stir welding T-joints of dissimilar aluminum alloys, *Journal of Materials Engineering and Performance*, 2012. **21**(8), 1763-1771.

16. Hugo Robe et al., Microstructural and mechanical characterization of a dissimilar friction stir welded butt joint made of AA2024-T3 and AA2198-T3, *Materials Characterization*, 2015.
17. D. Texier et al., Near-surface mechanical heterogeneities in a dissimilar aluminum alloys friction stir welded joint, *Materials & Design*, 2016. **108**, 217-229.
18. YN Zhang et al., Review of tools for friction stir welding and processing, *Canadian Metallurgical Quarterly*, 2012. **51**(3), 250-261.
19. Ákos Meilinger and Imre Török, The importance of friction stir welding tool, *Production Processes and Systems*, 2013. **6**(1), 25-34.
20. Emad Salari et al., Influence of tool geometry and rotational speed on mechanical properties and defect formation in friction stir lap welded 5456 aluminum alloy sheets, *Materials & Design*, 2014. **58**, 381-389.
21. Shude Ji et al., Design of friction stir welding tool for avoiding root flaws, *Materials*, 2013. **6**(12), 5870-5877.
22. LV Kamble, SN Soman, and PK Brahmankar, Effect of Tool Design and Process Variables on Mechanical Properties and Microstructure of AA6101-T6 Alloy Welded by Friction Stir Welding, *Journal of Mechanical and Civil Engineering (IOSR-JMCE)*, 2012.
23. I. Radisavljevic et al., Influence of FSW parameters on formation quality and mechanical properties of Al 2024-T351 butt welded joints, *Transactions of Nonferrous Metals Society of China*, 2013. **23**(12), 3525-3539.
24. G. Bussu and P. E. Irving, The role of residual stress and heat affected zone properties on fatigue crack propagation in friction stir welded 2024-T351 aluminium joints, *International Journal of Fatigue*, 2003. **25**(1), 77-88.
25. Jianqiang Chen et al., Plastic flow and ductile rupture of a 2198 Al–Cu–Li aluminum alloy, *Computational Materials Science*, 2011. **50**(4), 1365-1371.